Nature Environment and Pollution Technology
An International Quarterly Scientific Journal

p-ISSN: 0972-6268
(Print copies up to 2016)
e-ISSN: 2395-3454

Vol. 21 | No. 3 | pp. 1113-1123 | 2022

Original Research Paper

https://doi.org/10.46488/NEPT.2022.v21i03.016

Open Access Journal

Assessing the Capacities of Different Remote Sensors in Estimating Forest Stock Volume Based on High Precision Sample Plot Positioning and Random Forest Method

Yang Hu* and Zhongqiu Sun†**

*School of Ecology and Environment, Ningxia University, Yinchuan 750021, China

*Breeding Base for State Key Laboratory of Land Degradation and Ecological Restoration in Northwest China, Ningxia University, Yinchuan 750021, China

*Key Laboratory for Restoration and Reconstruction of Degraded Ecosystem in Northwest China of Ministry of Education, Ningxia University, Yinchuan 750021, China

**Academy of Inventory and Planning, National Forestry and Grassland Administration, Beijing 100714, China

†Corresponding author: Zhongqiu Sun; qiuqiu8708@163.com

Nat. Env. & Poll. Tech.
Website: www.neptjournal.com

Received: 20-07-2021
Revised: 25-09-2021
Accepted: 04-10-2021

Key Words:
Forest stock volume
Sentinel-1
Sentinel-2
Landsat-8
PALSAR2/PALSAR
Random forest

ABSTRACT

Forest stock volume (FSV) is an important forest resource indicator. Satellite images from various sensors have been used to estimate FSV. However, there is still a lack of comparative studies on the estimation of FSV with remote sensing data obtained by different sensors. In addition, there is a lack of high-precision ground sample positioning methods, which can improve the matching of ground data and remote sensing data to a certain extent, and improve the estimation accuracy. In this research, a new ground sample plot positioning method was proposed, which could achieve sub-meter positioning accuracy in forest areas, greatly improving the matching accuracy of ground sample plot data and remote sensing data. Based on this high-precision positioning method and the random forest algorithm, we compared and quantified the ability of different sensors to estimate the FSV. The results by random forest modeling showed that the images from a single sensor, Sentinel-2, performed best in the test dataset (R^2 = 0.57, RMSE = 70.12 m^3 ha^{-1}). For the data from two sensors, the best performance was achieved by the combined Sentinel-2 and PALSAR2/PALSAR data, which had an R^2 of 0.62 with RMSE of 65.51 m^3 ha^{-1} in the validation data. The images from the three sensors, Sentinel-2, Landsat-8, and PALSAR2/PALSAR, achieved a modeling accuracy of R^2 (0.62) and RMSE (65.40 m^3 ha^{-1}). The results clearly showed the capacity of the different sensor data to estimate FSV based on the high precision sample plot positioning method, and it will help forest researchers investigate and estimate the FSV in the future.

INTRODUCTION

As an important part of terrestrial ecosystems, forests play vital roles in both economic development and ecosystem protection. Forests are an important renewable natural resource that is crucial to the strategic timber security of a country (Xia et al. 2019). At the same time, forest ecosystems are the largest carbon pools in terrestrial ecosystems (Sun et al. 2020). Due to the close relationship between forests and carbon (Mitchard 2018), any change in forests directly impacts carbon sequestration (Zhang et al. 2020). Also, forest ecosystems play an irreplaceable role in ecosystems that includes absorbing carbon dioxide from the air, providing animal habitat, maintaining the carbon balance, and mitigating global climate. The management and monitoring of forests mainly require focusing on the information about wood resources, which can be assessed through the volume of trees, which is commonly known as the forest stock volume (FSV). Forest resource inventories are primarily conducted to estimate the existing FSV in forests, which has practical relevance for ecological environmental monitoring and sustainable forest management. Therefore, accurately assessing FSV at the regional and national scales is of great significance.

Currently, some studies have been performed based on a single sensor data or the combination of various sensor data for FSV estimation. For instance, Chrysafis et al. (2017) performed FSV estimation research using Sentinel-2 and Landsat-8 data in Greece. By modeling with the random forest (RF) algorithm, they obtained the best FSV prediction result with Sentinel-2 data (R^2 = 0.63, RMSE = 63.11 $m^3.ha^{-1}$). Muaya et al. (2019) estimated the FSV of a small-scale forest plantation in Tanzania with Sentinel-1(SAR), Sentinel-2, and ALOS PALSAR2 data with multiple linear regression

algorithms. They found that the Sentinel-2 data (RMSEr = 42.03%, pseudo-R^2 = 0.63) performed better than the combined Sentinel-1 and Sentinel-2 data (RMSEr = 46.98%, pseudo-R^2= 0.52), and Sentinel-1 performed worst (RMSEr = 59.48%, pseudo-R^2= 0.18). These studies showed that different data combinations had different forest parameter estimation results. Further research is needed to evaluate the feasibility and limitations of multi-sensor integrated datasets to estimate forest parameters (such as FSV). On the other hand, the complex collinearity among independent variables is an urgent problem during the process of model construction that cannot be avoided in traditional linear regression models, for example, some parametric methods. However, RF, which is a non-linear algorithm, could solve complex collinearity problems. Compared to the multiple regression algorithm, the resistance to collinearity and robustness to outliers of the RF algorithm make it uniquely feasible for predicting forest parameters using remote sensing variables (Breiman 2001).

In addition to remote sensing data and modeling algorithms, the importance of ground truth from sample plot data should not be ignored. However, the positioning accuracy of traditional handheld GPS units in forest areas is very low, and the error can even exceed 30 m (Stefanoni et al. 2018). Given the large position deviation in forests, it is necessary to find a positioning method to solve this problem. Huang et al. (2013) found that the accurate plot location recorded by DGPS (1-meter accuracy) reduced the geolocation error and thus achieved high prediction accuracy in the estimation of forest AGB (Huang et al. 2013).

This study has two objectives: (1) to test and determine a new forest sample plot positioning method that can achieve sub-meter accuracy in deep mountain forests and (2) to assess the performance of different sensor datasets (Sentinel-1, Sentinel-2, Landsat-8, and PALSAR2/PALSAR) in estimating FSV based on ground sample plots using the new positioning method. This paper will propose a new forest sample plot positioning method, clarify the performance of the yearly Sentinel-1, Sentinel-2, Landsat-8, and PALSAR2/PALSAR data in estimating the FSV in Southern China, especially Hunan Province, and even promote the estimation of FSV throughout the whole country.

MATERIALS AND METHODS

High-Precision Positioning Experimental Design

Three GNSS receivers produced by the Hi-Target Navigation Technology Corporation (H32 Almighty GNSS RTK System) were used in this experiment. A GNSS receiver was set up in a wide urban area, which ensured that the GNSS receiver could receive satellite signals well and use the continuously operating reference stations (CORS) service to achieve accurate positioning. The other two GNSS receivers were set up in the dense forest, in which the canopy density reached 0.7 or more. All three GNSS receivers worked together for 30 min at each designed distance (Fig. 1).

Measurement Accuracy Evaluation Method on Positioning

The CORS service was used in all GNSS receivers to obtain the coordinates $R\ (X_r, Y_r)$ as true positioning values. All GNSS receivers could also obtain the coordinates $E\ (X_e, Y_e)$ after the post-decomposition calculation. Then, equation (1) was used to calculate the D_{error}, which represented the positioning accuracy.

$$D_{error} = \sqrt{(X_r - X_e)^2 + (Y_r - Y_e)^2} \quad \ldots(1)$$

Sample Plot Data Collection

A total of 459 sample plots were investigated from October 1, 2017, to April 1, 2018, in Hunan province (Table 1, Fig. 2). The newly designed sample plot positioning method was used to position the individual tree and sample plot centers. The Vertex Laser VL5 was used to measure the tree heights. A DBH tape was used to measure the diameter at the breast height of the trees. All trees in the sample plots with DBHs greater than 5 cm were measured. The shape of the sample plot was a circle with a diameter of 30 m. The FSV of the sample plot was calculated (Hu et al. 2020) and extended to the hectare scale. To accurately match the remote sensing pixels, the sample plots were resampled to a cell size of 25 m × 25 m. To normally distribute the FSV data, the data were processed with a normal transformation function ($f(FSV) = FSV^{\lambda}$, λ =0.4) (Pan et al. 2019).

Landsat-8 Surface Reflectance Tier 1 Data

Landsat-8 Surface Reflectance Tier 1 data were available on the Google Earth Engine (GEE) platform. To match the date of our sample plot data and fully cover the research area, the date filter was set from May 1, 2017, to October 31, 2017, and May 1, 2018, to October 31, 2018. Clouds and cloud shadows were masked by the "pixel-qa" band. A "median" function was applied to extract the median value of all overlapping images, and seven characteristic spectral bands (e.g., B2, B3, B4, B5, B6, B7, B10) were finally calculated. All calculated bands were resampled to a 25 m resolution.

Sentinel-2 Level-1C Data

Sentinel-2 Level-1C product was used to extract the spectral characteristics, and the date filter was set from May 1, 2017, to October 31, 2017, and May 1, 2018, to Oct 31, 2018. Three

Table 1: Summary of normally transformed sample plots.

Forest types	Main species	Number of plots	FSV (m^3 ha^{-1})				
			Min	Max	Mean	Median	Std
Broadleaf forest	*Quercus, Cinnamomum camphora, Phoebe zhennan, Alniphyllum fortunei, Liquidambar formosana, Schima superba,* Gum trees, etc.	169	1.15	11.30	5.95	6.14	2.11
Needleleaf forest	*Cunninghamia lanceolata, Pinus massoniana, Cupressus funebris, Metasequoia glyptostroboides, Cryptomeria,* etc.	231	1.52	12.72	6.38	6.46	2.20
Mixed forest	*Cunninghamia lanceolata, Pinus massoniana, Cupressus funebris, Quercus, Cinnamomum camphora, Phoebe zhennan, Alniphyllum fortunei,* etc.	59	1.78	11.43	6.77	7.04	2.33

available bands were first used to mask the clouds in the images. The QA60 band is a cloud mask band that is used to mask opaque clouds with a threshold setting of less than 1. Then, the B1 band was used to mask cirrus clouds with a threshold setting of less than 1500. The B2 band was used to mask cirrus clouds with a threshold setting of greater than 2500. After that, the "median" function was used to extract pixel values. Eleven bands were calculated (i.e., B2, B3, B4, B5, B6, B7, B8, B8A, B10, B11, B12), and all bands were resampled to a 25 m resolution.

Global PALSAR2/PALSAR Data

The global 25 m PALSAR2/PALSAR mosaic data are available from January 1, 2007, to January 1, 2018, on the GEE

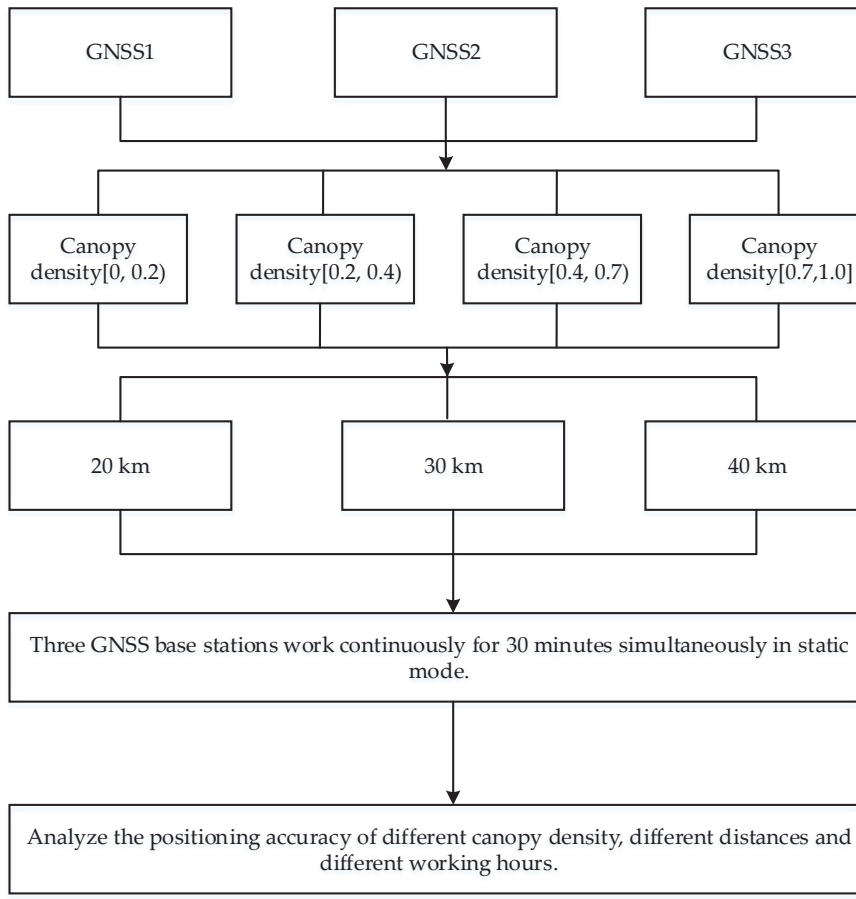

Fig. 1: Flowchart of the GNSS positioning experiment.

platform. The 2017 yearly mosaic data was used to match our sample plot data. The HH and HV bands were selected and processed in windows of different sizes (1 ×1 pixel, 3 ×3 pixels, 5 ×5 pixels, 7 ×7 pixels, 9 ×9 pixels, 11 ×11 pixels, 13 ×13 pixels). Then, equation (2) was used to convert the DN values to gamma naught values in decibel units (dB) (Qin et al. 2017).

$$\gamma^0 = 10\log_{10}\mathrm{DN}^2 - 83.0\ \mathrm{dB} \quad \ldots(2)$$

Sentinel-1 SAR Data

The Sentinel-1 SAR ground range detected (GRD) dataset has data that starts on October 3, 2014, on the GEE platform; the further data processing was conducted based on the research of Hird et al. (2017), including (1) masking the edges of the images using the angle; (2) filtering out windy days using climate forecasts; (3) performing angle correction; and (4) filtering with different windows (1 × 1 pixel, 3 × 3 pixels, 5 × 5 pixels, 7 × 7 pixels, 9 × 9 pixels, 11 × 11 pixels, 13 × 13 pixels).

RF Regression Algorithm

The RF regression algorithm is a popular regression algorithm in this field of study. It uses the bootstrap method to generate multiple datasets to build multiple decision trees (regression trees). The average of the predicted values of the multiple decision trees is used as the final output of the RF regression model. The RF regression model can be mathematically summarized as follows: given a data sample X and a prediction set Y, a forest-dependent on the random variable θ is planted on this basis to form a tree predictor $h(X, \theta_k)$, which outputs the result as a numerical value. The RF predictor is obtained by averaging these trees $\{h(X, \theta_k)\}$ with respect to k (k represents the number of sub-training datasets). The RF regression function is as follows: $Y = E_\theta h(X, \theta_k)$. The out-of-bag (OOB) data was used to calculate the prediction error (PE) of each regression tree (Equation (3)).

$$\mathrm{PE} = E_\theta E_{X,Y}(Y - h(X, \theta_k))^2 \quad \ldots(3)$$

The principle of the RF regression is as follows (Fig. 3):

In the model development (number = 321, ratio = 0.7) and model test (number = 138, ratio = 0.3), the performance of each RF model was evaluated by the coefficient of determination (R^2) and root mean square error (RMSE) (Wang et al. 2019).

$$R^2 = \frac{\sum_{i=1}^{m}(f_i - \bar{y})^2}{\sum_{i=1}^{m}(y_i - \bar{y})^2} \quad \ldots(4)$$

$$\mathrm{RMSE} = \sqrt{\frac{1}{m}\sum_{i=1}^{m}(y_i - f_i)^2} \quad \ldots(5)$$

Where f_i is the modeling predictor; y_i is the measured value of the sample plot; $\bar{y}$ is the mean measured value of the sample plot; and m is the number of training and test data points.

Variable Selection

Variable selection is necessary when modeling with a large number of independent variables. It simplified the models, shortens the training times, breaks the curse of dimensionality, and enhances the generalization by reducing over-fitting. In this study, the "VSURF" package in R 3.5.3 was used to select variables for different data combinations (Genuer et al. 2015).

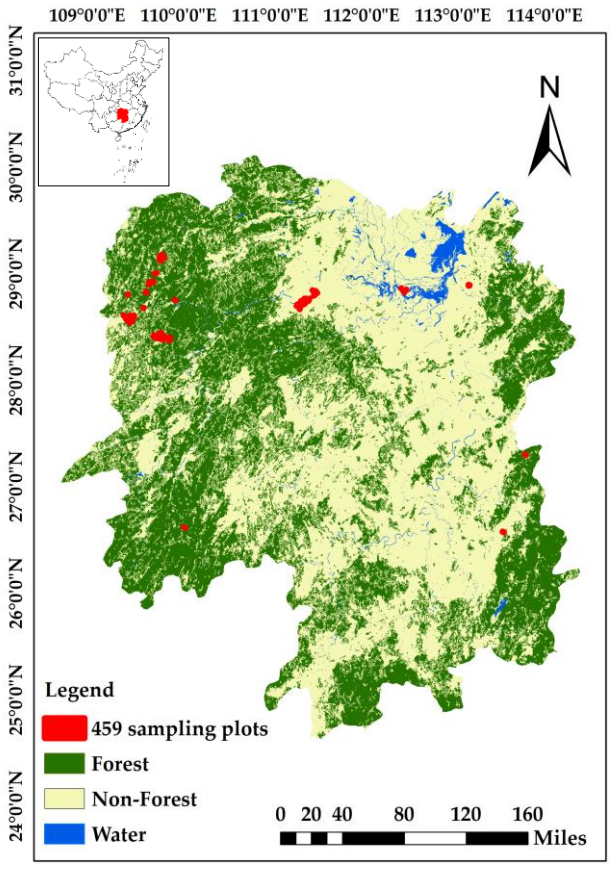

Fig. 2: Sample plots spatial distribution in Hunan, China.

RESULTS

The Newly Designed Differential Positioning Accuracies

Through the static relative positioning test under different distances, different times, and different stand environments, it can be concluded that distance, time, and forest stand environment all have different effects on the positioning accuracy

(Fig. 4). Under the forest stand conditions of the first canopy density level, the GNSS receiver can reach a positioning accuracy of 0.50 m within a static range of 30 km for 10 minutes. However, under the second canopy density forest stand condition, the static duration of more than 25 min at a distance of 30 km is required to achieve a positioning accuracy of 0.50 m. Under the third canopy density forest stand conditions, at least 20 minutes of the static state is required at a distance of 30 km.

Selection of Variables for Image Classification

For the Sentinel-1 and PALSAR2/PALSAR variables, only 2 variables (HH, VV) were included in each window size, and the variable selection step was not conducted. The preprocessing step was performed first to decide which window size had a stronger relationship with the FSV. However, considering the weak performance of the Sentinel-1 data, we only selected the PALSAR2/PALSAR variables of 11×11 window size to estimate the FSV.

The "VSURF" package was used for the Sentinel-2 and Landsat-8 variables. For the Sentinel-2 variables, 5 out of 11 variables were selected: blue band (B2), green band (B3), red band (B4), red edge 1 band (B5), and SWIR 1 band (B11). In Landsat-8 variables, 6 out of 9 variables were selected: ultra-blue band (B1), green band (B3), red band (B4), near-infrared band (B5), shortwave infrared-2 band (B7), and brightness temperature band (B11). The variable combinations for all cases are summarized in Table 2.

FSV Estimation with the RF Regression Model

For the training data, Fig. 5 shows the performance of different data combinations in the training phase. The best performance was the data combination with Sentinel-2, Landsat-8, and PALSAR2/PALSAR, with the highest $R^2 = 0.94$ and the lowest RMSE = 32.19 $m^3.ha^{-1}$. The worst performance was the PALSAR2/PALSAR (except Sentinel-1), with the lowest $R^2 = 0.86$ and the largest RMSE = 47.75 $m^3.ha^{-1}$.

For the test data, Fig. 6 shows the performance of different data combinations in the test phase. The best performance was also the combined Sentinel-2, Landsat-8, and PALSAR2/PALSAR data, which had the highest R^2(0.62) and the lowest RMSE (65.40 $m^3.ha^{-1}$). The worst performance was the PALSAR2/PALSAR (except Sentinel-1), which had the lowest $R^2 = 0.25$ and the largest RMSE = 81.87 $m^3.ha^{-1}$.

Table 2: The selected variables for RF modeling.

Sensor(s)	Variable selection												
P11	H11	V11											
S2	S2_B2	S2_B3	S2_B4	S2_B5	S2_B11								
L8	L8_B1	L8_B3	L8_B4	L8_B5	L8_B7	L8_B11							
S2+P11	S2_B2	S2_B3	S2_B4	S2_B5	S2_B11	H11	V11						
L8+P11	L8_B1	L8_B3	L8_B4	L8_B5	L8_B7	L8_B11	H11	V11					
S2+L8	S2_B2	S2_B3	S2_B4	S2_B5	S2_B11	L8_B1	L8_B3	L8_B4	L8_B5	L8_B7	L8_B11		
S2+ L8+P11	S2_B2	S2_B3	S2_B4	S2_B5	S2_B11	L8_B1	L8_B3	L8_B4	L8_B5	L8_B7	L8_B11	H11	V11

Note: S2 stands for Sentinel-2, L8 stands for Landsat-8, P11 stands for PALSAR2/PALSAR in an 11×11 window size, and H11 stands for HH in an 11×11 window size, and V11 stands for HH in an 11×11 window size.

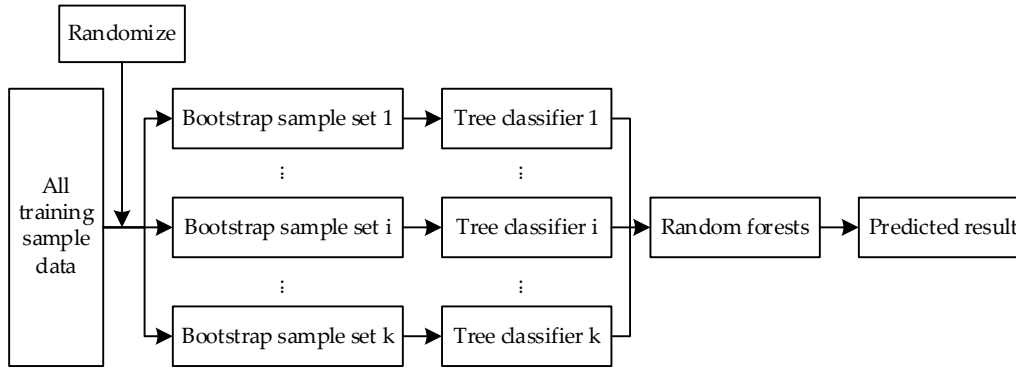

Fig. 3: Flowchart of the RF principle.

DISCUSSION

The Potential Of Multi-Sensor Image Data to Improve FSV Estimation

For the Sentinel-1 SAR data, the performance of FSV estimation was very poor. A similar study also found that the Sentinel-1 SAR data did not perform well in estimating FSV, with an R^2 of only 0.18 (Mauya et al. 2019). The main reason for the poor performance may be the saturation problem (Huang et al. 2018). Since the SAR-C band is easily affected by speckle noise in complex forests, some studies have only used Sentinel-1 SAR on grass fields (Crabbe et al. 2019).

When considering the L-band PALSAR2/PALSAR dataset, it performed slightly better than the SAR-C band dataset because the PALSAR2/PALSAR L-band dataset had a higher saturation than the Sentinel-1 SAR-C band dataset in estimating FSV. However, it still did not perform well. Some studies also showed that the ALOS PALSAR data did not perform well in forest biomass estimation (Zhao et al. 2016). Saturation is a major cause of poor performance. Some studies have also found that saturation problems could occur in some forest areas using ALOS PALSAR data to estimate FSV (Antropov et al. 2013). In our sample plot data, the sample values ranged from 1.42 $m^3.ha^{-1}$ to 577.49 $m^3.ha^{-1}$, and many sample values were under 100 $m^3.ha^{-1}$, which may be the main reason for our poor modeling result.

For the single dataset, Sentinel-2 performed best both in the training phase and test phase, which showed that the

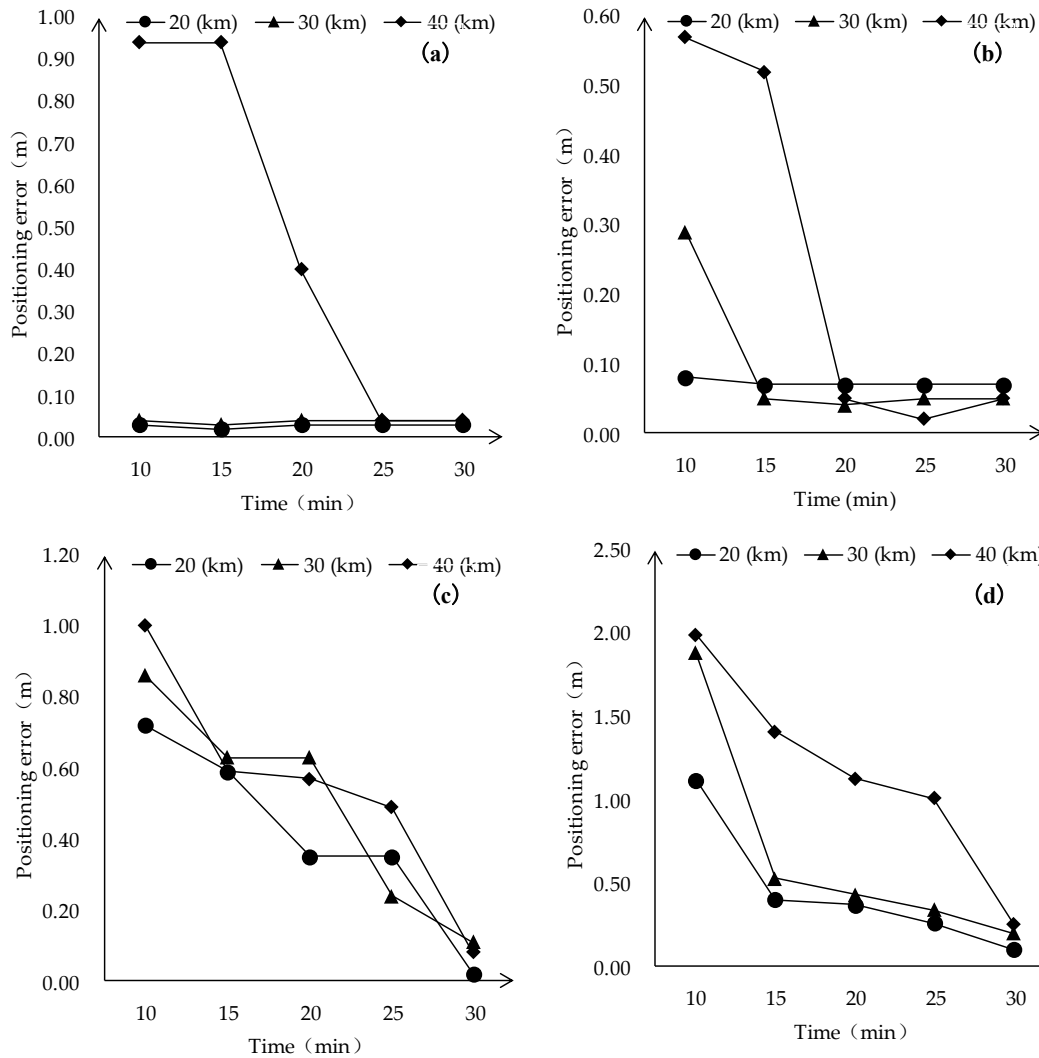

Fig. 4: Static relative positioning error at different distances, different times, and different forest environments: (a) non-forest area, (b)the first canopy density level forest area, (c) the second canopy density level forest area, and (d) the third canopy density level forest area.

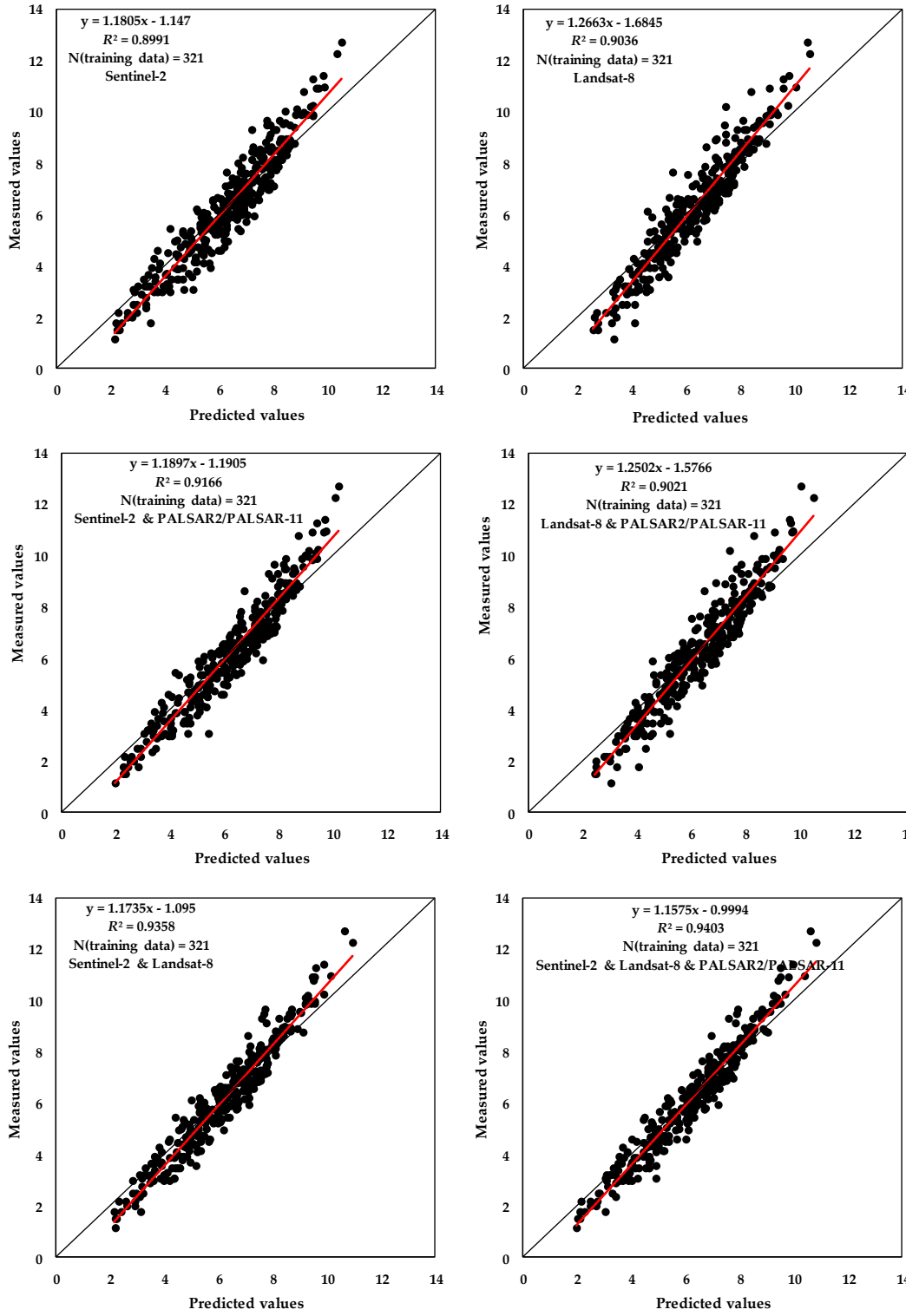

Fig. 5: The performance of the different sensors in the training phase.

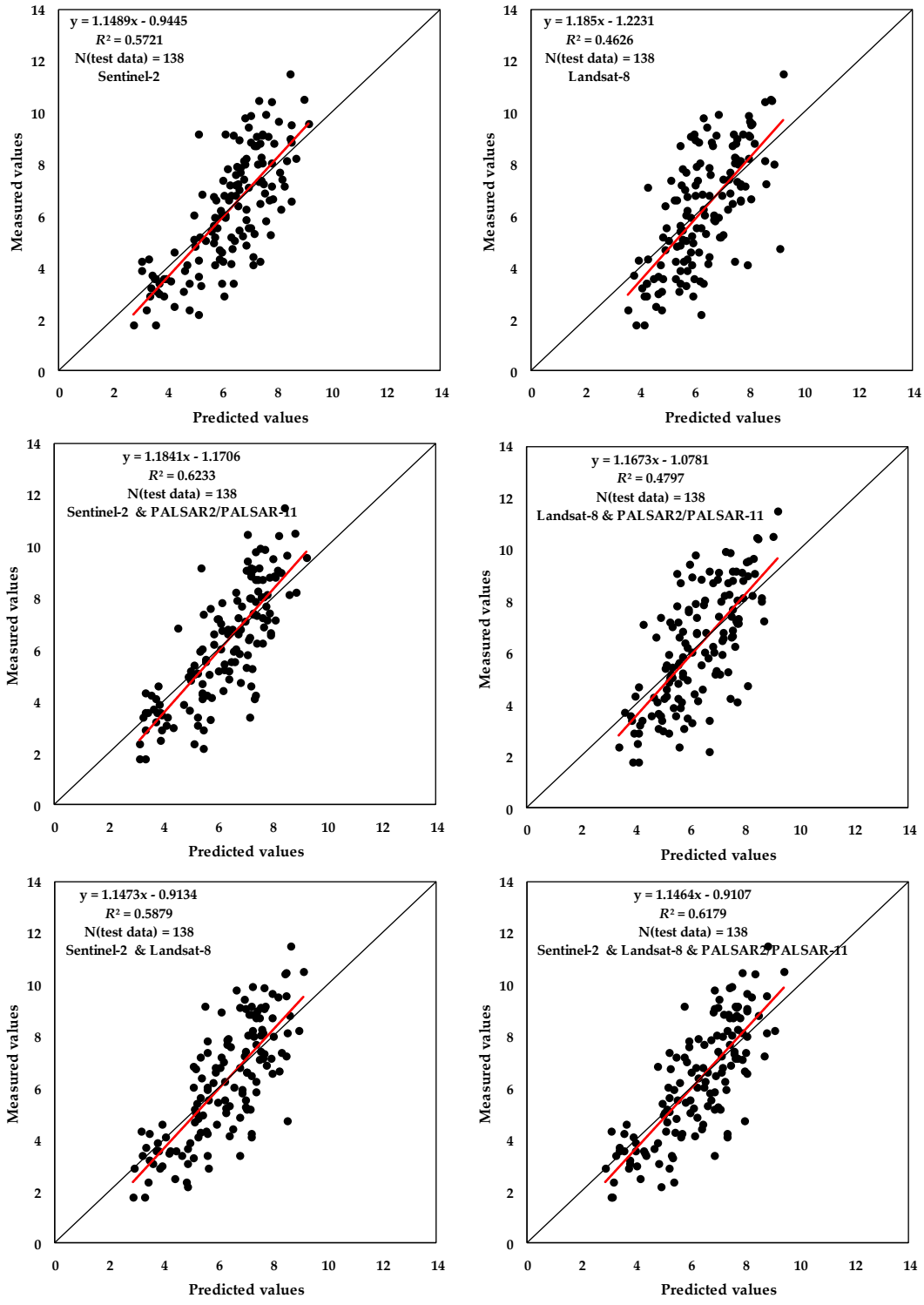

Fig. 6: The performance of different sensors in the test phase.

Sentinel-2 dataset was more appropriate than the Landsat-8 dataset, with B5 (red edge 1) possibly having a positive effect on the FSV estimation. Some studies have proven that the red edge information was related to FSV and biomass estimation (Vaglio et al. 2014). For the data combination, although the combined Sentinel-2, Landsat-8, and PALSAR2/PALSAR data performed best, the Sentinel-2 and PALSAR2/PALSAR datasets performed only slightly worse than the three data combinations. The combined Landsat-8 and PALSAR2/PALSAR data not only had the worst performance among the data combinations but also performed worse than the Sentinel-2 data. This showed that it was unnecessary to use Landsat-8 data when Sentinel-2 data was being used to estimate FSV. Additionally, adding PALSAR2/PALSAR may only create a small level of positive feedback for FSV estimation.

Although the fusion of the three data sources improved the prediction performance under the RF regression model, the test accuracy was still not high. This was caused by the saturation of the data. In forestland with a small FSV, sparse trees and bare ground directly impact the spectral and microwave signals, which affects the accuracy of modeling. Spectral unmixing may be a way to improve the modeling accuracy (Lu et al. 2005). In forestland with a high FSV, optical image and microwave signal saturation were the main reasons leading to the decline in the prediction model's performance. To date, there has been no effective way to solve the saturation problem caused by the data itself (Lu et al. 2016). However, some studies have found that the LiDAR data performed quite well in the forest research field based on its unique ability to penetrate the canopy (Hu et al. 2019).

Potential of Machine Learning Methods and High-Quality In-Situ Data to Improve FSV Estimation

To achieve such modeling results in a large mountain area in Southern China with a large range of sample values, two points should be considered to achieve the ambitious goals of the study. The first point is the optimized RF algorithm. The best parameters (mtry, ntree) were calculated first to build the regression trees, which may have improved the accuracy of the regression model prediction. With some studies using default values (mtry is $\sqrt{n}$ or $\frac{n}{3}$, n is the number of modeling variables; ntree is 500 or 1000) for RF modeling, we calculated the two parameters using the MSE as a criterion, which would reduce the modeling time and improve modeling accuracy. Although the RF algorithm has been widely used and demonstrated to work quite well in comparison with other machine learning methods, deep learning methods should not be ignored. Some studies have used different deep learning methods to estimate forest parameters (Zhang et al. 2019). Based on this, additional research should also be conducted in the future.

The second point is the advanced sample positioning technology used in this research. Three GNSS receivers formed a triangulation model and one GNSS receiver was set in the urban area using the CORS service, which allowed it to obtain accurate coordinates as control points to correct the coordinates of the other two GNSS receivers, the positioning accuracy reached the sub-meter level. Compared with the traditional sample positioning method, this new positioning method would help match sample plots with the pixels of remote sensing images more accurately (Hu et al. 2019).

Likely Sources of Uncertainty in FSV Estimations

In this study, we acknowledge that the Sentinel-2 TOA data was not the best choice for FSV estimation. Although we extracted cloudless images, some factors, such as aerosols, will still have a certain effect on the reflectivity of the ground objects. However, processing the Sentinel-2 TOA data to BOA data at provincial or even national scales is unrealistic. The large volume of data would take a researcher several months or even years to complete on a local computer. Many studies have been conducted and demonstrated that it was acceptable to use TOA data to estimate forest parameters (Lin et al. 2015) and those for wetlands (Hird et al. 2017). However, we still recommend using Sentinel-2 BOA data to carry out research when BOA data are available in the future.

The sample plot data was another source of uncertainty in the FSV estimations. The uncertainty of sample data collection came from the measurement of the trees, the sample plot size, and the tree volume formula (Gao et al. 2018). The measurements of the trees mainly included tree height and DBH, which are directly related to the tree volume and therefore directly related to the FSV of the sample plot. The sample plots used in this study were circle plots with a diameter of 30 m, which was different from the resampling pixel size of remote sensing data. Although the FSV was calculated based on the size of the area and the center position of the plot, since pixels and sample plots were not directly matched, some errors will inevitably occur. This problem could be solved quite well by setting up large-area sample plots and using the pixel coordinates to directly extract the tree volumes in the plots. For the tree volume formula, not all tree species have corresponding calculation equations. Tree volume calculation through tree species classification will also have a certain impact on the original volume value. In addition, if the sample plot data are sufficient and follow

a normal distribution, the prediction accuracy of the model may be further improved (Mohd et al. 2018).

CONCLUSION

In this study, a new positioning method was proposed to obtain the center coordinates of sample plots and achieved an accuracy within 0.5 m. The sample plots were used to assess the capacity of the different sensor datasets to estimate FSV. Finally, the results showed that the Sentinel-1 SAR data and PALSAR2/PALSAR data was not suitable for estimating FSV in Southern China. However, the PALSAR2/PALSAR data could provide positive feedback when combined with other sensor data. Although the combined Sentinel-2, Landsat-8, and PALSAR2/PALSAR data performed best, the combination performed only slightly better than the combined Sentinel-2 and PALSAR2/PALSAR data. The third best performance was the Sentinel-2 data, which had a performance that was very close to that of the combined Sentinel-2 and PALSAR2/PALSAR data. Using Sentinel-2 data to estimate FSV is a good choice on a provincial scale. Combining Landsat-8 and PALSAR2/PALSAR data could not greatly improve the accuracy of the estimation. We will attempt to use LiDAR data and deep learning methods to estimate FSV in the future.

ACKNOWLEDGEMENT

This work was funded by the Natural Science Foundation of Ningxia Province (Grant number 2021AAC03017), and the Ningxia Key Research and Development Project (2018BFG02015). The authors are grateful to the Chinese Academy of Inventory and Planning, and the National Forestry and Grassland Administration, for providing the in situ data used in this study.

R1EFERENCES

Antropov, O., Rauste, Y., Ahola, H. and Hame, T. 2013. Stand-level stem volume of boreal forests from spaceborne SAR imagery at L-Band. IEEE J. Sel. Topics Appl. Earth Observ. Remote Sens., 6(1): 35-44.

Breiman, L. 2001. Random forests. Mach. Learn., 45: 5-32.

Chrysafis, M., Siachalou, R. and Patias, M. 2017. Assessing the relationships between growing stock volume and Sentinel-2 imagery in a Mediterranean forest ecosystem. Remote Sens. Lett., 8(6): 508-517.

Crabbe, R.A., Lamb, D.W., Edwards, C., Andersson, K. and Schneider, D. 2019. A preliminary investigation of the potential of Sentinel-1 radar to estimate pasture biomass in a grazed, native pasture landscape. Remote Sens., 11(7): 872.

Gao, Y., Lu, D., Li, G., Wang, G., Chen, Q., Liu, L. and Li D. 2018. Comparative analysis of modeling algorithms for forest aboveground biomass estimation in a subtropical region. Remote Sens., 10(4): 627.

Genuer, R., Poggi, J. and Tuleau-Malot, C. 2015. VSURF: An R package for variable selection using random forests. R J., 7(2): 19-33.

Hird, J., H., Evan, D.L., Gregory, M.D. and Jahan, K. 2017. Google earth engine, open-access satellite data, and machine learning in support of large-area probabilistic wetland mapping. Remote Sens., 9(12): 1315.

Hu, Y., Wu, F. Sun, Z., Andrew, L., Gao X., Li, W. and Peng D. 2019. the laser vegetation detecting sensor: a full waveform, large-footprint, airborne laser altimeter for monitoring forest resources. Sensors, 19(7): 35-63.

Hu, Y., Xu, X., Wu, F., Sun, Z., Hung, W., Meng, Q., Peng, D. and Xiao, X. 2020. Estimating forest stock volume in Hunan Province, China, by Integrating with situ plot data, Sentinel-2 images, and linear and machine learning regression models. Remote Sens., 12(1): 186.

Huang, W., Sun, G., Dubayah, R., Cook, B., Montesano, P. and Ni, W. 2013. Mapping biomass change after forest disturbance: Applying LiDAR footprint-derived models at key map scales. Remote Sens. Environ., 134: 319-332.

Huang, X., Ziniti, B., Torbick, N. and Ducey, M. 2018. Assessment of forest above-ground biomass estimation using multi-temporal C-band Sentinel-1 and Polarimetric L-band PALSAR-2 Data. Remote Sens., 10(9): 1424.

Lin, C., Popescu, S.C., Gavin, T., Khongor, T., Chang, C.I. and Prasad, V.K. 2015. Classification of tree species in overstorey canopy of the subtropical forest using quick bird images. PLoS One, 10(5): e125554.

Lu, D., Batistella, M. and Moran E. 2005. Satellite estimation of aboveground biomass and impacts of forest stand structure. Photogr. Eng. Remote Sens., 71(8): 967-974.

Lu, D., Chen, Q., Wang, G., Liu, L., Li, G., and Emilio, M. 2016. A survey of remote sensing-based aboveground biomass estimation methods in forest ecosystems. Int. J. Digital Earth, 9(1): 63-105.

Mauya, E.W., Koskinen, J., Tegel, K., Hmlinen, J. and Kyhk, N. 2019. Modeling and predicting the growing stock volume in small-scale plantation forests of Tanzania using multi-sensor image synergy. Forests, 10(3): 279.

Mitchard, T.A. 2018. The tropical forest carbon cycle and climate change. Nature, 559(7715): 527-534.

Mohd, N.A., Latif, Z.A. and Suratman, M.N. 2018. Modeling above-ground live trees biomass and carbon stock estimation of tropical lowland Dipterocarp forest: Integration of field-based and remotely sensed estimates. Int. J. Remote Sens., 39(8): 2312-2340.

Pan, P., Sun, Y., Ouyang, X., Zang, R. and Zhang, N. 2019. Factors affecting spatial variation in vegetation carbon density in Pinus massoniana lamb: Forest in subtropical China. Forests, 10(10): 88

Qin, Y., Xiao, X., Dong, J., Zhou, Y. and Moore, B. 2017. Annual dynamics of forest areas in South America during 2007–2010 at 50-m spatial resolution. Remote Sens. Environ., 201: 73-87.

Stefanoni, H., Reyes-Palomeque, G., Castillo-Santiago, M., George-Chacón, S., Huechacona-Ruiz, A. and Tun-Dzul, F. 2018. Effects of sample plot size and GPS location errors on aboveground biomass estimates from LiDAR in tropical dry forests. Remote Sens., 10(10): 1586.

Sun, W. and Liu, X. 2020. Review on carbon storage estimation of forest ecosystem and applications in China. Forest Ecosyst., 7(1): 1-14.

Vaglio, L.G, Qi, C., Lindsell, J.A., Coomes, D.A., Frate, F.D., Guerriero, L., Pirotti, F. and Valentini, R. 2014. Above-ground biomass estimation in an African tropical forest with lidar and hyperspectral data[J]. ISPRS J. Photogr. Remote Sens., 89: 49-58.

Wang, J., Xiao, X., Bajgain, R., Starks, P. and Chang, Q. 2019. Estimating leaf area index and aboveground biomass of grazing pastures using Sentinel-1, Sentinel-2, and Landsat images[J]. ISPRS J. Photogr. Remote Sens., 154: 189-201.

Xia, H., Qin, Y., Feng, G., Meng, Q. and Liu, G. 2019. Forest phenology dynamics to climate change and topography in a geographic and

climate transition zone: The Qinling mountains in Central China. Forests, 10(11): 1007.

Yu, Z., Ji, Y., Cy, B., Rui, C., Bo, T. B. and Han, L. B. 2020. Contributions of national key forestry ecology projects to the forest vegetation carbon storage in China. Forest Ecol. Manag., 462: 117981.

Zhang, L., Shao, Z., Liu, J. and Cheng, Q. 2019. Deep learning-based retrieval of forest aboveground biomass from combined LiDAR and Landsat 8 Data. Remote Sens., 11(12): 1459.

Zhao, P., Lu, D., Wang, G., Liu, L., Li, D., Zhu, J. and Yu, S. 2016. Forest aboveground biomass estimation in Zhejiang Province using the integration of Landsat TM and ALOS PALSAR data. Int. J. Appl. Earth Observ. Geoinform., 53: 1-15.